GSICS Global Space-based Inter-Calibration System

# Quarterly

Newsletter Summer 2021 Issue

doi: 10.25923/w710-y903
Vol. 15 No 2, 2021
Editor: Manik Bali, ESSIC/UMD

CMA • CNES • ESA • EUMETSAT • IMD • ISRO • JAXA • JMA • KMA • NASA • NIST • NOAA • ROSCOSMOS • ROSHYDROMET • SITP • USGS • WMO

## Articles



## News in This Quarter



## Announcements



## GSICS Related Publications

# 10 years of satellite infrared radiance monitoring with the Met Office model

*By Roger Saunders, Pete Francis, Tom Blackmore, Brett Candy (Met Office) and Tim Hewison (EUMETSAT)*

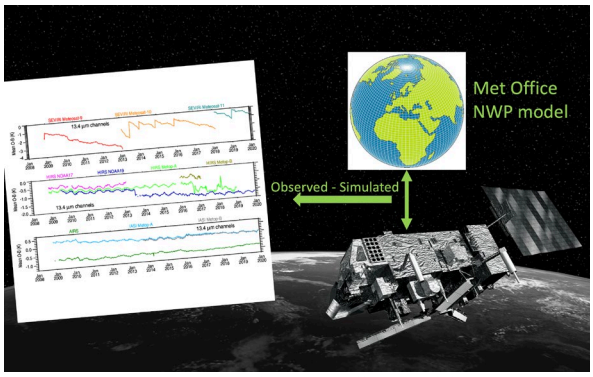


*Image curtsey R. Saunders depicts Satellite- Model Intercomparison*

Using the Met Office global Numerical Weather Prediction (NWP) model, over 10 years of meteorological satellite imagery and sounder clear sky infrared radiances have been continuously monitored to show the stability of these instruments with time. This provides valuable information to produce fundamental climate data records (FCDRs) and also for assimilation in reanalyses. The details are described in a recent paper [1] in addition to a more detailed analysis over a shorter period reported earlier in [2]. A brief review of some of the results of the 10 years' timeseries are reported here.

Three infrared wavelengths were chosen to assess the instruments which were monitored listed in Table 1. They were the 'window' infrared channel at 10.8µm, the water vapour channel at 6.7µm and the carbon dioxide channel at 14.2µm (13.4µm for Meteosat/SEVIRI). Using a fast radiative transfer model (RTTOV) [3], the clear sky radiances were simulated from the NWP model temperature, water vapour and surface fields. The observed minus model simulated differences (hereafter referred to as O-B) for each channel were averaged over the Meteosat full disk area or globally in this study. The period over which each instrument was monitored, channel numbers and source of the data are also listed in Table 1.

For IASI on Metop-A, Metop-B and Metop-C the mean O-B values are virtually the same for all three instruments and channels (see Figures 1 and 2 for the 10.8µm and 6.7µm channels) and are stable throughout the 2013-2019 time period. The standard deviation of the O-B values for the IASI water vapour channels (not shown) shows a decrease over the 10 years demonstrating an improved representation of the upper tropospheric water vapour fields in the Met Office model. The mean bias of the water vapour channels for all the infrared sensors has become more positive with time due to a moistening of the NWP model's upper tropospheric humidity.

AIRS radiances have also been stable over the 10-year period but have mean biases typically 0.5 K warmer than IASI which may be related to the radiative transfer model or a diurnally varying bias of the model fields as both instruments sample the diurnal cycle at different times of the day. There is also a small positive trend when compared with the IASI O-B values. This analysis also includes a short period of ENVISAT AATSR radiances [4], which

doi: 10.25923/w710-y903



has a refined on-board calibration system and shows a mean difference in between AIRS and IASI for its 10.8µm channel. The IASI and AIRS radiance measurements will make good FCDRs as they are shown to be stable and have only small biases when compared to global NWP simulations.

The HIRS instruments, designed many years ago, exhibit somewhat larger but stable biases until the filter wheel jitter occurs and then the O-B values and standard deviation change significantly rendering the instrument unsuitable for use for periods as illustrated in Figures 1 and 2. In some cases after a bias change the instrument does settle down and then can be used again. The HIRS on Metop-B is in this category but for this processing it was removed when it became anomalous. Another complication with HIRS is that the overpass times-of-day drift with time potentially causing slowly changing O-B values. Clearly the HIRS radiances will need more care to produce stable FCDRs due to changes in instrument performance over time but given the long time series of HIRS radiances (back to the mid-1970s) it is a valuable dataset.

| Geostationary Satellite | Instrument | Channel Numbers | Source | Period |
|---|---|---|---|---|
| Meteosat-9 | SEVIRI | 5,9,11 | EUMETCAST | 19 Nov 2008-21 Jan 2013 |
| Meteosat-10 | SEVIRI | 5,9,11 | EUMETCAST | 21 Jan 2013-20 Feb 2018 |
| Meteosat-11 | SEVIRI | 5,9,11 | EUMETCAST | 20 Feb 2018-31 Dec 2019 |
| **Polar-orbit Satellite** | **Instrument** | **Channels** | **Source** | **Period** |
| Metop-A | IASI | 246, 1133, 3522 | EUMETCAST | 19 Nov 2008 – 31 Dec 2019 |
| | HIRS | 4,8,12 | EUMETCAST | 19 Nov 2008 – 31 Dec 2019 |
| Metop-B | IASI | 246, 1133, 3522 | EUMETCAST | 15 Sep 2013 – 31 Dec 2019 |
| | HIRS | 4,8,12 | EUMETCAST | 1 Jan 2016 – 16 Feb 2017 |
| Metop-C | IASI | 246, 1133, 3522 | EUMETCAST | 1 May 2019 – 31 Dec 2019 |
| Aqua | AIRS | 198, 787, 1756 | NESDIS | 19 Nov 2008 – 31 Dec 2019 |
| NOAA-17 | HIRS | 4,8,12 | NESDIS | 19 Nov 2008 –30 Jan 2013 |
| NOAA-19 | HIRS | 4,8,12 | NESDIS | 14 July 2009 – 31 Dec 2019 |
| ENVISAT | AATSR | 2 | FTP ESRIN | 1 Sep 2010 – 8 April 2012 |

**Table 1.** Instruments and channels for which bias monitoring statistics were collected during 2009-2019

Finally, for the SEVIRI imager on Meteosat the window and water vapour channels are reasonably stable over time and between different platforms (Figures 1 and 2) but the $CO_2$ channel bias (not shown) varies rapidly as ice builds up on the detector and is then removed by a decontamination procedure which reduces the bias by 2K. This can be difficult to accurately correct for and will make the FCDR generation for the SEVIRI 13.4µm channel challenging.

This kind of radiance monitoring is carried out in real time by the NWP Satellite Application Facility https://nwp-saf.eumetsat.int/site/monitoring/nrt-monitoring/ where O-B timeseries from several different NWP centres are plotted. This can be used to quickly

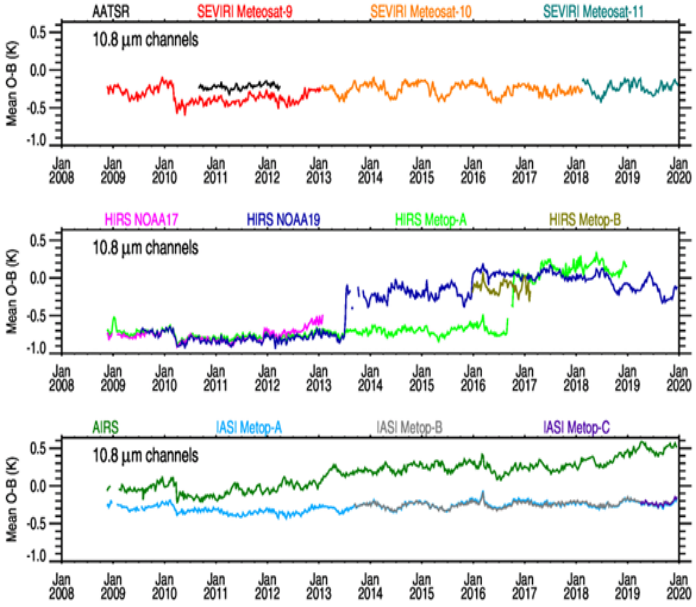


**Figure 1**. Time series of observed-background Meteosat, IASI, AIRS, AATSR and HIRS radiances for the 10.8 micron window infrared channels showing the mean over the Meteosat full disk area.

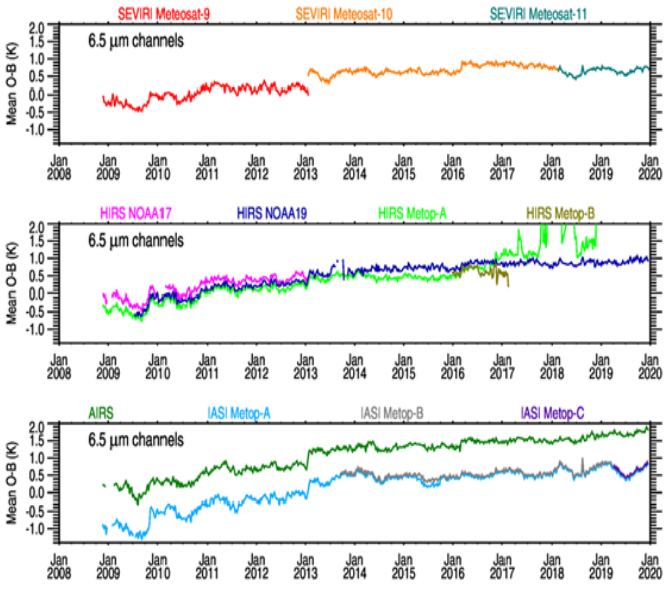


**Figure 2**. Time series of observed-background Meteosat, IASI, AIRS and HIRS radiances for the 6.5 micron water vapour channels over the Meteosat full disk area.

doi: 10.25923/w710-y903



identify problems with the instruments many of which are used for assimilating the radiances into NWP model analyses.

**Acknowledgments**

The satellite data were provided by EUMETSAT, ESA and NOAA as part of the real time delivery of data to the Met Office for operational data assimilation.

**Glossary**

AATSR – Advanced Along Track Scanning Radiometer
AIRS – Atmospheric Infra-Red Sounder
FCDR – Fundamental Climate Data Record
HIRS – High resolution Infrared Sounder
IASI – Infrared Atmospheric Sounding Interferometer Metop – Meteorological Operational satellite
RTTOV – Radiative Transfer for TOVS (a fast radiative transfer model)
SEVIRI – Spinning Enhanced Visible and Infrared Imager

**References**

[1] Saunders, R.W., T. A. Blackmore, B. Candy, P. N. Francis and T. J. Hewison, "Ten Years of Satellite Infrared Radiance Monitoring With the Met Office NWP Model," in IEEE Transactions on Geoscience and Remote Sensing, 59, no. 6, pp. 4561-4569, June 2021, doi: 10.1109/TGRS.2020.3015257.

[2] Saunders, R.W., T. A. Blackmore, B. Candy, P.N. Francis and T.J. Hewison. Monitoring satellite radiance biases using NWP models, IEEE Trans. Geosci. Remote Sens., vol. 51, no. 3, March 2013. doi:10.1109/TGRS.2012.2229283.

[3] Saunders, R.W., Hocking, J., Turner, E., Rayer, P., Rundle, D., Brunel, P., Vidot, J., Roquet, P., Matricardi, M., Geer, A., Bormann, N., and Lupu, C.: An update on the RTTOV fast radiative transfer model (currently at version 12). Geosci. Model Dev., 11, 2717–2737, 2018 https://doi.org/10.5194/gmd-11-2717-2018.

[4] Merchant, C., D. Llewellyn-Jones, R. Saunders, N. Rayner, E. Kent, C. Old, D. Berry, A. Birks, T. Blackmore, G. Corlett. Deriving a sea surface temperature record suitable for climate change research from the along-track scanning radiometers. Advances in Space Research vol. 41 (1), pp. 1–11, 2008.

# Consistent usage of a reference solar spectrum for establishing radiometric harmonization across multi-sensor L1B datasets

*By Rajendra Bhatt (NASA-LaRC), David Doelling (NASA-LaRC), and Odele Coddington (LASP)*

Most modern satellite remote sensing imagers (MODIS, VIIRS, ABI, etc.) are equipped with an on-board Solar Diffuser (SD) for obtaining in-flight radiometric calibration of the Earth-observation data. Based on prelaunch characterization, the SD provides a reference for reflectance-based calibration of the satellite-measured counts, which are later tied to a reference Solar Spectral Irradiance (SSI) dataset to derive the L1B dataset radiances. The choice of reference SSI spectrum for satellite data processing has changed as the accuracy of the SSI measurements improved. Earlier Landsat and AVHRR missions used the solar spectrum reported by Neckel and Labs [1]. The MODIS ground processing system implements a composite of three different SSI datasets: Thuillier et al. (1998) [2] for wavelengths between 350-800 nm, Neckel and Labs (1984) [1] between 800-1100 nm, and Smith and Gottlieb (1974) [3] between 1100-2500 nm. The VIIRS sensor on board NOAA-20 and SNPP spacecrafts sensor rely on Thuillier 2003 [4] and Kurucz MODTRAN 4.0 [5], [6] spectra, respectively, for deriving their L1B radiance datasets. Previous studies [7]–[10] have reported noticeable differences between these solar spectra that can potentially lead to incompatible retrievals from these satellite datasets.

| Name | Description | Uncertainty (%) |
|---|---|---|
| TSIS-1 SIM | Measured by TSIS-1 SIM instrument on ISS | 0.24-0.41% |
| HSRS | Hybrid Solar Reference Spectrum (HSRS) derived by normalizing the high-resolution solar line data to the absolute irradiance scale of the TSIS-1 SIM and CSIM instruments | 0.3-1.3% |
| Thuillier 2003 | Measured by SOLSPEC and SOSP spectrometers from ATLAS and EURECA missions | 1-3% |
| Kurucz (MODTRAN 4.0) | A theoretical spectrum of the solar continuum supplemented with observed and predicted solar lines | NA |
| MCST | Combination of Thuillier 1998, Neckel and Labs, and Smith and Gottlieb used by the MODIS Characterization and Support Team (MCST) for processing the MODIS L1B datasets | 2-3% |
| SOLAR-ISS V2 | Based on SOLAR/SOLSPEC spectroradiometer on ISS supplemented with observed and predicted solar lines | ~1.26% |
| WHI 2008 | Derived for the 2008 Whole Heliosphere Interval (WHI) using a combination of temporally coincident satellite and sounding rocket observations | 3% |

**Table 1:** List of solar spectra used in this study and their uncertainties.

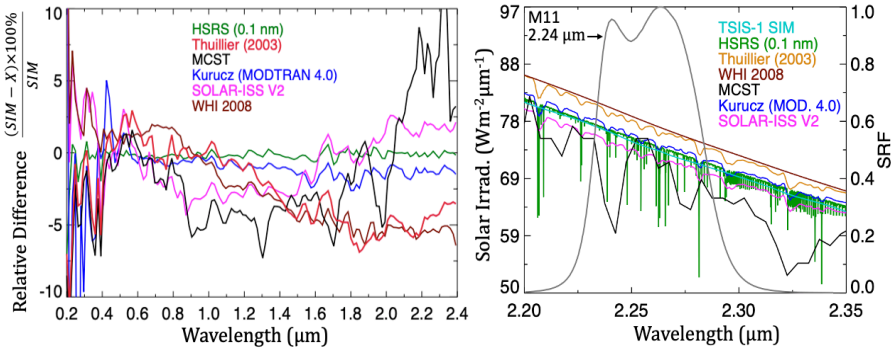


**Figure 1:** (Left) Relative difference of individual solar spectra computed with respect to the TSIS-1 SIM spectrum as a function of wavelength. (Right) SRF of NOAA-20 VIIRS M11 band along with various solar spectra shown in the background.

doi: 10.25923/w710-y903



Recently, Bhatt et al. [11] performed a comprehensive analysis of absolute comparison between the most commonly used SSI datasets (Table 1) [4], [5], [12]–[15], and quantified their impacts in satellite inter-calibration. Fig.1(left) shows relative difference of these spectra (at comparable spectral resolution) with respect to the TSIS-1 SIM spectra, which has the best-known radiometric precision and accuracy (<0.5%). The TSIS-1 Hybrid Solar Reference Spectrum (HSRS), a composite spectrum developed by normalizing fine spectral resolution solar line observations to the high-accuracy TSIS-1 SIM absolute irradiance scale, agrees within ~1% for wavelengths between 400-2400 nm. The Kurucz solar spectrum exhibits differences more than 5% at shorter wavelengths and up to ~2.5% in SWIR regimes. The Thuillier 2003 spectrum is consistent with the TSIS-1 SIM measurements within ~2.5% in VIS and NIR wavelengths. However, the difference nearly exceeds +7% for SWIR wavelengths. The greatest relative difference (>10%) is found for the MCST spectra near 2.3 µm. It is noteworthy to mention that the observed differences between these spectra exceed their reported uncertainties [11].

Fig. 1 (right panel) shows the SRF of NOAA-20 VIIRS M11 (2.25 µm) along with the various solar spectra. The band-integrated solar constant ($E_{SUN}$) is derived by convolving a solar spectrum with the SRF. A percentage difference in the $E_{SUN}$ value is computed for each of the spectra relative to the Thuillier 2003 spectra. These differences are listed in Table 2 for the VIIRS reflective solar bands. A negative percentage difference indicates the radiances would be greater compared to using the Thuillier 2003 spectra. Because the two VIIRS sensors use different solar spectra, the magnitude of radiometric biases between the two VIIRS instruments are different for their radiance and reflectance datasets. For example, if the two VIIRS I1 band reflectances were perfectly calibrated, their radiances can still differ by 1.64%. The maximum difference in the $E_{SUN}$ value is computed for the M11 band, where these spectra exhibit the greatest discrepancy. A consistent difference of ~1.4% between the MCST (based on Thuillier 1998) and Thuillier 2003 spectra for wavelengths less than 0.8 µm (highlighted by a red box in Table 2) is due to the fact that the latter incorporates a 1.4% wavelength-independent normalization to match the then adopted TSI value of 1368 W/m$^2$ [4].

| NOAA20 VIIRS band | Difference in $E_{sun}$ relative to Thuillier (%) | | | | | |
|---|---|---|---|---|---|---|
| | MCST | TSIS-1 SIM | HSRS (0.1 nm) | Kurucz (MODTRAN) | SOLAR ISS v2 | WHI 2009 |
| M1 (0.41 µm) | -1.40 | -0.54 | -0.51 | -0.08 | -2.28 | 0.81 |
| M2 (0.45 µm) | -1.41 | -0.61 | -0.56 | 2.09 | -1.71 | 0.78 |
| M3 (0.49 µm) | -1.40 | -0.78 | -0.78 | -0.48 | -1.54 | 0.15 |
| M4 (0.56 µm) | -1.40 | -2.26 | -2.06 | -2.06 | -1.33 | -1.02 |
| M5 (0.67 µm) | -1.44 | -0.98 | -1.40 | -1.64 | -1.15 | 0.54 |
| I1 (0.64 µm) | -1.43 | -0.95 | -1.30 | -1.42 | -2.0 | 0.42 |
| M6 (0.75 µm) | -1.40 | 0.41 | 0.25 | -0.24 | -1.95 | 2.12 |
| M7 (0.87 µm) | -2.71 | 0.12 | 0.18 | 0.11 | -3.23 | 0.65 |
| M8 (1.24 µm) | -4.33 | 0.88 | 0.77 | -0.19 | -1.39 | -1.45 |
| M9 (1.38 µm) | -0.56 | 2.48 | 2.35 | 1.62 | 0.12 | -0.75 |
| M10 (1.61 µm) | 1.11 | 3.96 | 3.60 | 2.18 | 2.99 | -0.45 |
| M11 (2.25 µm) | 10.23 | 4.14 | 4.11 | 2.89 | 6.00 | -1.01 |

**Table 2:** Percentage difference in $E_{SUN}$ values for NOAA-20 VIIRS channels computed for various solar spectra relative to the Thuillier 2003 spectra.

The existing non-uniformity in the usage of reference solar spectra among the multiple satellites L1B radiance datasets adds extra challenges to achieve radiometric harmonization across the sensors. It is feasible to reverse engineer the L1B radiance dataset to get rid of the embedded solar spectrum and incorporate a common reference SSI but this is only possible if the solar spectra used is documented. The GSICS VIS/NIR sub-group recommends using TSIS-1 HSRS as a common reference solar spectrum for use in the calibration of current and future RSB satellite instruments due to its excellent absolute accuracy and high spectral resolution [16].

## References


[1] H. Neckel and D. Labs, "The solar radiation between 3300 and 12500 Å," *Sol. Phys.*, vol. 90, no. 2, pp. 205–258, 1984.

[2] G. Thuillier *et al.*, "The visible solar spectral irradiance from 350 to 850 nm as measured by the solspec spectrometer during the ATLAS I mission," *Sol. Phys.*, vol. 177, no. 1–2, pp. 41–61, 1998.

[3] E. V. P. Smith and D. M. Gottlieb, "Solar flux and its variations," *Space Sci. Rev.*, vol. 16, no. 5–6, pp. 771–802, 1974.

[4] G. Thuillier *et al.*, "The solar spectral irradiance from 200 to 2400 nm as measured by the SOLSPEC spectrometer from the ATLAS and EURECA missions," *Sol. Phys.*, vol. 214, no. 1, pp. 1–22, 2003.

[5] R. L. Kurucz, "The solar irradiance by computation," in *Proceedings of the 17th Annual Conference on atmospheric transmission models*, 1995, vol. 95, pp. 333–334.

[6] A. Berk *et al.*, "MODTRAN4 radiative transfer modeling for atmospheric correction," in

doi: 10.25923/w710-y903



*Optical Spectroscopic Techniques and Instrumentation for Atmospheric and Space Research III*, 1999.

[7] L. Zhang, S. Hu, H. Yang, T. Wu, Q. Tong, and F. Zhang, "The effects of solar irradiance spectra on calculation of narrow band top-of-atmosphere reflectance," *IEEE J. Sel. Top. Appl. Earth Obs. Remote Sens.*, vol. 7, no. 1, pp. 49–58, 2014.

[8] P. Shanmugam and Y. H. Ahn, "Reference solar irradiance spectra and consequences of their disparities in remote sensing of the ocean colour," *Ann. Geophys.*, vol. 25, no. 6, pp. 1235–1252, 2007.

[9] S. Uprety, C. Cao, S. Blonski, and X. Shao, "Assessing the NOAA-20 and S-NPP VIIRS radiometric consistency," 2018, p. 32.

[10] R. Bhatt, D. R. Doelling, C. Haney, D. A. Spangenberg, B. Scarino, and A. Gopalan, "Clouds and the Earth's Radiant Energy System strategy for intercalibrating the new-generation geostationary visible imagers," *J. Appl. Remote Sens.*, vol. 14, no. 03, p. 1, 2020.

[11] R. Bhatt, D. R. Doelling, O. Coddington, B. Scarino, A. Gopalan, and C. Haney, "Quantifying the impact of solar spectra on the inter-calibration of satellite instruments," *Remote Sens.*, vol. 13, no. 8, 2021.

[12] O. M. Coddington *et al.*, "The TSIS-1 Hybrid Solar Reference Spectrum," *Geophys. Res. Lett.*, vol. Submitted, 2020.

[13] E. Richard *et al.*, "SI-traceable spectral irradiance radiometric characterization and absolute calibration of the TSIS-1 spectral irradiance monitor (SIM)," *Remote Sens.*, vol. 12, no. 11, 2020.

[14] M. Meftah *et al.*, "A New Version of the SOLAR-ISS Spectrum Covering the 165 – 3000 nm Spectral Region," *Sol. Phys.*, vol. 295, no. 2, 2020.

[15] T. N. Woods *et al.*, "Solar Irradiance Reference Spectra (SIRS) for the 2008 Whole Heliosphere Interval (WHI)," *Geophys. Res. Lett.*, vol. 36, no. 1, 2009.

[16] T. Stone, O. Coddington, J. Bak, and D. Doelling, "Vis/NIR subgroup proposes TSIS-1 HSRS as the GSICS recommended solar spectrum," *GSICS Q. Newsl.*

# OLCI A/B tandem phase analysis: a summary

*By Nicolas Lamquin, Alexis Déru, Sébastien Clerc, Ludovic Bourg (ACRI-ST) and Craig Donlon (ESA/ESTEC)*

## Introduction

The operational Sentinel-3 setting includes two identical satellites providing global observations daily at the same equator crossing time. Shortly after its launch, the Sentinel-3B satellite was maneuvered into a four-month tandem configuration with its twin Sentinel-3A already in orbit [1], providing a unique opportunity to increase knowledge of payload differences, to homogenize datasets by defining appropriate adjustments, and to reduce uncertainties when comparing data [2].

This article summarizes the outcomes of the ESA Sentinel-3 for Climate study (https://s3tandem.eu) with respect to the Ocean and Land Colour Instrument (OLCI) [3]. Despite sharing the same industrial design, OLCI-A and OLCI-B do not share the same exact spectral characterization nor radiometric and geometric calibrations. The tandem phase is an ideal setup to investigate the impact of these differences and perform the necessary adjustments to homogenize and harmonize the two series of measurement.

**Table 1:** Mean and median relative differences (%) between harmonized OLCI-A and OLCI-B L2 products.

| Quantity | OGVI | OTCI | nRrs 400 | nRrs 412 | nRrs 443 | nRrs 490 | nRrs 510 | nRrs 560 | Chl |
|---|---|---|---|---|---|---|---|---|---|
| Mean relative difference (%) | 0.7 | -1.2 | -0.4 | -1.2 | 0.3 | 0.9 | 1.0 | 1.6 | 4.0 |
| Median relative difference (%) | 0.0 | -1.0 | -0.3 | -1.4 | -0.8 | 0.6 | 0.7 | 1.1 | 3.0 |

doi: 10.25923/w710-y903



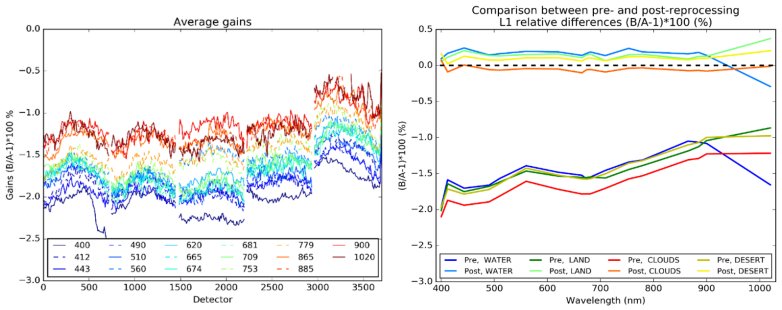


**Figure 1.** Left: Raw cross-calibration factors between OLCI-A and OLCI-B across the OLCI Field-of-View ("Detector") and per wavelength (each line). Right: summary statistics per target type and per wavelength of the raw L1 radiometric differences (after homogenization) pre- and post-harmonization.

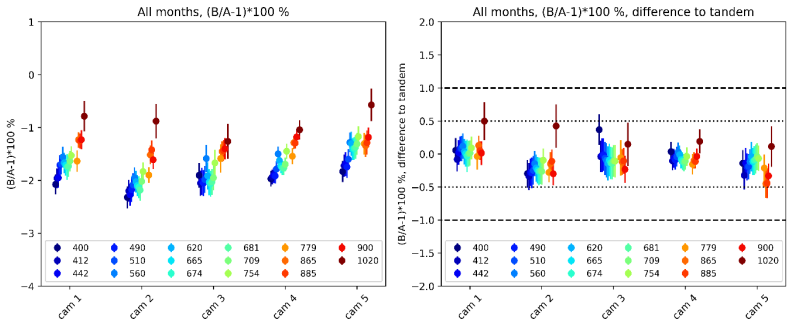


**Figure 2.** Left: per-camera mean and associated standard deviation of the DCC methodology for all OLCI bands over the period Nov 2019 / May 2020. Right: comparisons to the tandem analysis cross-calibration factors.

Analyses of L1 products first allow us assess a methodology for the homogenization and the radiometric harmonization of OLCI-A and OLCI-B [4]. Analyses of L2 and L3 products then highlight benefits and limitations of the harmonization separately for land and water products [5,6]. Finally, tandem and post-tandem acquisitions are used to investigate and validate a new methodology based on Deep Convective Clouds (DCC) for monitoring the cross-calibration of OLCI-A and OLCI-B over the mission lifetime [7].

### Homogenization and harmonization

Analyses of the L1 products validates a homogenization and harmonization methodology of OLCI-A and OLCI-B L1B TOA radiances [4]. The homogenization process is scene-dependent to account for the spectral specificities of the type of target, higher quality being found from comparisons over cloudy targets. Evidence of a 1 to 2% bias (Figure 1, left) confirm reporting from radiometric validation activities [8], the tandem configuration providing better precision and accuracy.

By compensating for these biases (Figure 1, right), harmonization provides a radiometric alignment better than 0.5% across the full OLCI spectrum (strong absorption bands are not considered though). Further analyses also highlight inter-camera radiometric biases, up to 1.5%, similarly in OLCI-A and OLCI-B.

### Benefits on L2 products

Analyses of the subsequent L2 products, confirm that harmonization currently provides the best reachable alignment of the L2 products [5]. Statistics are recapitulated in Table 1.

For Land products, the benefit for the OLCI Global Vegetation Index (OGVI) has proven very significant whereas persistent differences (pre and post harmonization) in the OLCI Terrestrial Color Index (OTCI) underline a lack of accuracy in the spectral adjustment of the red-edge band (709 nm).

For Water products, the alignment of L2 water-leaving reflectance (expressed as normalized remote sensing reflectance, nRrs) and Chlorophyll (Chl) are provided with excellent accuracy compared to the mission requirements, paving the way for a joint vicarious calibration of harmonized OLCI products against ground-truth measurements.
As for L1 products, it appeared that L2 products would potentially benefit from the equalization of the OLCI cameras, differences in water-leaving reflectance up to 10% between two adjacent cameras being cancelled after applying equalization [5].

We stress that inter-camera calibration differences may impact accuracy and precision of vicarious calibration, and, generally, of radiometric validation.

### Post-tandem cross-calibration monitoring

Analyses of tandem and post-tandem L1 products over Deep Convective Clouds (DCCs) allows us develop and validate a methodology [7] for monitoring OLCI-A/B cross-calibration. Its basic concepts can be generalized to future OLCI sensors as well as other series of optical sensors.
This methodology is based on a statistical analysis over monthly to multi-monthly DCC observations sampled across the OLCI FOV. A main methodological finding is the use of the inflexion point of DCC reflectance probability distributions. This indicator provides the ability to monitor the cross-calibration of the two sensors with accuracy better than 1% on a monthly basis, even better than 0.5% from multi-monthly statistics (Figure 2). Results indicate that the OLCI-A/B radiometric biases observed from the tandem phase products persist after tandem (within the precision of the method), to the exception of the 1020 nm band for which a correction of saturated pixels in OLCI-A is less accurate, and to the exception of the 400 nm band camera 3

which indeed suggests slight calibration changes in both OLCI sensors (see details in [7]).The method also provides a confirmation as well as a quantification of OLCI inter-camera radiometric biases.

## Conclusions

The Sentinel-3A/B tandem phase provided ideal conditions to bypass stronger spectral, radiometric, and geometric differences usually faced in cross-sensor comparisons as well as procuring out-performing statistics. Focusing on OLCI, a homogenization and harmonization methodology provides evidence of biases between the OLCI-A and -B sensors as well within each of the instrument's cameras. Benefits of harmonization as well as equalization have been assessed for L1 and L2 products.
Although main analyses and results were obtained from the tandem products, a novel methodology based on statistics of Deep Convective Clouds observations is shown to be able to monitor the cross-calibration of the OLCI out of tandem. Radiometric differences between OLCI-A and OLCI-B are shown to be stable over time, which remains to be carefully monitored in the future for the application of harmonization over the mission lifetime. We strongly support the use of tandem phases for future optical sensors (e.g. next OLCI-C and -D, Sentinel-2, FLEX/OLCI…) and stress that this unique approach should be the normal approach to fill needs of key users such as the GCOS and the Copernicus Climate Change Service.

## References

1. Donlon, C. J.; O'Carroll, A.; Smith, D.; Scharroo, R.; Bourg, L.; Kwiatkowska, E.; Merchant, C.; Sathyendranath, S.; Labroue, S.; Larnicol, G. Scientific Justification for a Tandem mission between Sentinel-3A and Sentinel-3B during the E1 commissioning Phase, European Space Agency Technical Note EOP-SM/3057/CD-cd, Issue 4.3, available form the European Space Agency, Noordwijk, The Netherlands. 2017.
2. Clerc, S.; Donlon, C.; Borde, F.; Lamquin, N.; Hunt, S.E.; Smith, D.; McMillan, M.; Mittaz, J.; Woolliams, E.; Hammond, M.; Banks, C.; Moreau, T.; Picard, B.; Raynal, M.; Rieu, P.; Guérou, A. Benefits and Lessons Learned from the Sentinel-3 Tandem Phase. Remote Sens. 2020, 12, 2668. https://doi.org/10.3390/rs12172668 .
3. Nieke, J.; Borde, F.; Mavrocordatos, C.; Berruti, B.; Delclaud, Y.; Riti, J.-B.; Garnier, T. The Ocean and Land Colour Imager (OLCI) for the Sentinel 3 GMES Mission: status and first test results. Proc. SPIE 8528, Earth Observing Missions and Sensors: Development, Implementation, and Characterization II, 85280C (28 November 2012), https://doi.org/10.1117/12.977247.
4. Lamquin, N.; Clerc, S.; Bourg, L.; Donlon, C. OLCI A/B tandem phase analysis, part 1: Level 1 homogenisation and harmonisation. *Remote Sens.* 2020, 12(11), 1804, https://doi.org/10.3390/rs12111804 .
5. Lamquin, N.; Déru, A.; Clerc, S.; Bourg, L.; Donlon, C. OLCI A/B Tandem Phase Analysis, Part 2: Benefits of Sensors Harmonisation for Level 2 Products. Remote Sens. 2020, 12, 2702. https://doi.org/10.3390/rs12172702 .
6. Hammond, M.L.; Henson, S.A.; Lamquin, N.; Clerc, S.; Donlon, C. Assessing the Effect of Tandem Phase Sentinel-3 OLCI Sensor Uncertainty on the Estimation of Potential Ocean Chlorophyll-*a* Trends. *Remote Sens.* **2020**, *12*, 2522. https://doi.org/10.3390/rs12162522 .
7. Lamquin, N.; Bourg, L.; Clerc, S.; Donlon, C. OLCI A/B Tandem Phase Analysis, Part 3: Post-Tandem Monitoring of Cross-Calibration from Statistics of Deep Convective Clouds Observations. *Remote Sens.* **2020**, *12*, 3105. https://doi.org/10.3390/rs12183105 .
8. Bourg, L.; Blanot, L.; Alhammoud, B.; Sterck, S.; Preusker, R. Sentinel-3 A and B OLCI instruments Calibration Status. Proceedings of the Fifth Sentinel-3 Validation Team Meeting, 2019.

## Acknowledgement

This work has been performed under the European Space Agency Science and Society Contract 4000124211/18/I-EF. We thank the S3TC and ACRI-ST teams, the S3-Mission Performance Center, and EUMETSAT for the provision of OLCI data. The first author would like to express his gratitude to Dave Doelling for his review of the present summary as well as to the GSICS community for welcoming and broadcasting this work.

doi: 10.25923/w710-y903



# Calibration and Characterization of Satellite-Borne Microwave Sounders with the Moon

*By Martin Burgdorf, University of Hamburg*

**Introduction:** A major problem with calculating the uncertainties of measurements with weather satellites is the fact that a full characterization and calibration of their instruments can only be carried out before launch. The Moon, however, makes at least some of these activities possible in flight as well by providing a reliable flux reference at a well-defined position. We used serendipitous observations of the Moon with AMSU-B (Advanced Microwave Sounding Unit-B) and MHS (Microwave Humidity Sounder) on eight different satellites to measure pointing accuracy, spectral channels co-registration, and beam width with unprecedented accuracy in flight. Once the geometric performance was characterized, we took advantage of this knowledge for calculating the flux from the Moon.

**Spectral Channels Co-registration and Pointing Accuracy:** In order to check the absolute pointing accuracy of AMSU-B and MHS, we selected intrusion events in which the Moon came closer than 0.05° to the center of the deep space view according to the pointing information in the Level 1b Records. We identified more than 13 of such cases for each satellite, except for METOP-C, which was launched later than the others. The results are shown in Figure 1. $\phi$ is the azimuth (across track direction) and $\theta$ is the elevation (approximately along track direction); the origin for both angles is the direction given in the Level 1b Records. The nominal beam pointing accuracy is ±0.1° for either axis of AMSU-B and ±0.09° for MHS. The antenna requirement for channels co-registration is ±0.07° for MHS. The pointing error we determined in flight is more than a factor of two worse than allowed by the requirements for AMSU-B on NOAA-17 and MHS on METOP-C, but the co-registration is almost always compliant with the requirements.

**Mean Half Power Beam Width:** We determined the beam width from the period of time that the signal stays above half the maximum value in the light curve of a Moon intrusion in the DSV. The results from our investigation are summarized in Table 1. The requirement for beam width is 1.1° ± 0.11° for AMSU-B and MHS. When the beam widths are significantly larger than 1.21°, that is, outside the amount allowed by the requirement, they are printed in boldface.

**Brightness Temperature of the Moon:** With the careful characterization of the geometric properties of the instruments, we are now in a position to use the amplitude of the light curves to determine the relationship between brightness temperature, averaged over the lunar disk, and phase angle. As the observations of the Moon with MHS on NOAA-18 covered the range from first quarter to full Moon almost completely, this satellite is particularly well suited for this purpose, see Figure 2. As the distance between the Sun and the Moon varies slightly because of the eccentricity of the Earth's orbit, the actual direct solar irradiance at the Moon fluctuates by about 6.9 % during a year. This influences its brightness temperature, which was corrected for in Figure 2.

**Table 1: Mean Half Power Beam width of AMSU-B on NOAA-15 - NOAA-17 and MHS on NOAA-18, NOAA-19, and Metop From Ground Tests (Subscript "gr") and in Orbit (Subscript "op").**

| Satellite | $89_{gr}$ | $89_{op}$ | $150/157_{gr}$ | $150/157_{op}$ | $183_{gr}$ | $183_{op}$ | $190_{gr}$ | $190_{op}$ |
|---|---|---|---|---|---|---|---|---|
| N 15 | 1.12 | 1.199±0.005 | 1.03 | **1.293±0.011** | 1.05 | 1.207±0.006 | | |
| N 16 | 1.12 | 1.212±0.006 | 1.05 | **1.338±0.014** | 1.08 | 1.227±0.009 | | |
| N 17 | 1.16 | 1.210±0.010 | 1.00 | **1.239±0.010** | 1.00 | 1.093±0.007 | | |
| N 18 | 1.09 | 1.172±0.004 | 1.03 | 1.067±0.006 | 1.05 | 1.221±0.004 | 1.05 | **1.241±0.005** |
| N 19 | 1.10 | 1.178±0.003 | 1.15 | 1.141±0.003 | 1.12 | **1.271±0.008** | 1.12 | **1.260±0.003** |
| M A | 1.11 | 1.177±0.036 | 1.17 | 1.158±0.037 | 1.07 | 1.215±0.025 | 1.08 | 1.263±0.041 |
| M B | | 1.120±0.031 | | 1.066±0.029 | | 1.140±0.021 | | 1.182±0.033 |
| M C | | 1.245±0.066 | | 1.223±0.062 | | 1.278±0.050 | | 1.308±0.073 |

doi: 10.25923/w710-y903



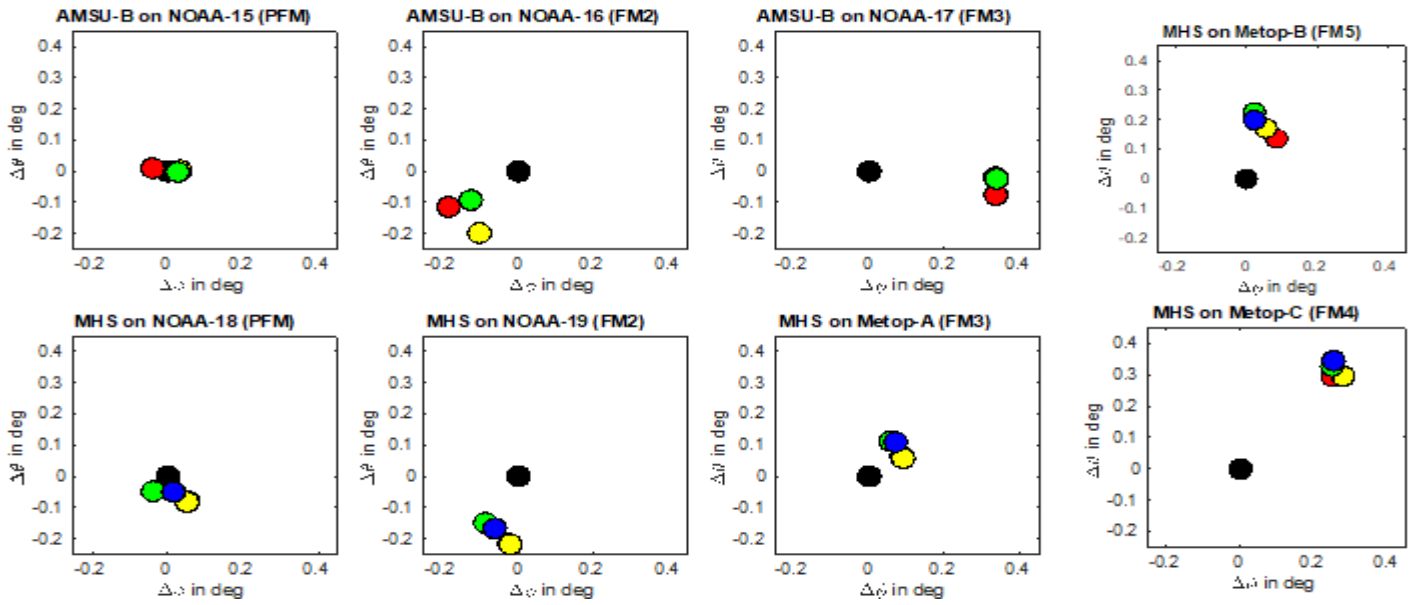


**Figure 1**. In-flight pointing performance showing the co-registration of the channels 16/H1 (89 GHz, red), 17/H2 (150/157 GHz, yellow), 18–20/H3-4 (183 GHz, green, only channel H4 with NOAA-19), and H5 (190 GHz, blue) at the space view. $\Delta\phi$ is the error in across track direction, $\Delta\vartheta$ is the error in the along track direction. The black circle indicates the nominal pointing direction; yellow is sometimes on top of red and green on top of yellow. 0.1° corresponds to about 1.5 km at the subsatellite point. PFM means Proto-Flight Model, and FM means Flight Model. Compare to the results from ground tests in https://www-cdn.eumetsat.int/files/2020-05/pdf_mhs_char_data_des.pdf

**Conclusions:** Comparing the results we obtained for the pointing accuracy and beam width in flight with those from the tests before launch, one finds significant discrepancies. In particular, the pointing of MHS on METOP-C and to a lesser extent on METOP-B and NOAA-19 is off the mark in the across scan direction, and the beam width of the sounding channels is always a bit on the high side. We double checked our unexpectedly high values for the beam width with a quite different method, based on their impact on calculating the measured flux from the Moon, so we are certain they are right. The ground tests carried out by Airbus Defense and Space, by contrast, are conspicuous by their strong tendency to err on the side of better compliance with the requirements. For details see https://doi.org/10.1029/2021EA001725

Figure 2 shows that Liu's model fits the changes of the measured brightness temperature of the Moon as a function of phase angle very well. The discrepancy between models and observations with respect to the absolute flux level of the lunar disk at mm-wavelengths can be due to incorrect input to the models or systematic uncertainties in the calibration of MHS. For climate studies, however, flux trends matter more than the absolute flux level, and our investigation suggests that Liu's model can predict brightness variations of the Moon with an accuracy better than one percent. Hence the Moon is actually a more reliable flux reference at microwaves than in the visible part of the spectrum

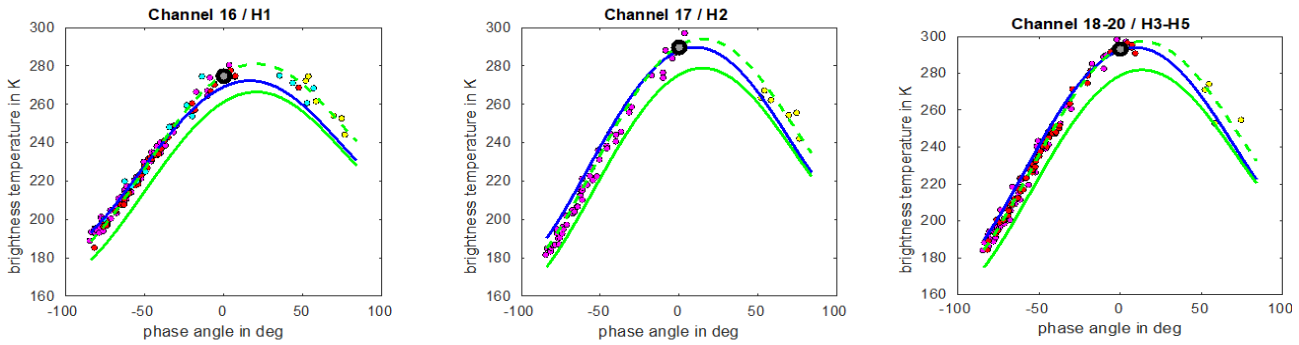


**Figure 2.** Brightness temperatures of the lunar disk from measurements at 89 GHz with AMSU-B on NOAA-16 (cyan) and NOAA-17 (yellow) and with MHS on NOAA-18 (red) and NOAA-19 (magenta), at 150 GHz with AMSU-B on NOAA-17 and at 157 GHz with MHS on NOAA-19, and as well with AMSU-B on NOAA-17 at 183.3 GHz and MHS on NOAA-18 and NOAA-19 with the average of the 183.3 and 190.3 GHz channels. The gray circle stands for ATMS on NOAA-20 (Yang et al., 2020) at the same frequencies, except for 165~GHz instead of 150 or 157 GHz. The blue line represents the brightness temperatures predicted by the model by Keihm (1984), and the solid, green line represents the model by Liu and Jin (2020). The latter model has also been scaled to higher brightness temperatures, the result is shown as the dashed, green line. Compare to the situation at visible wavelengths on slide 30 of https://drive.google.com/drive/folders/1WoCXYPppDevjRKzPROhVqfp_D9kDxoMD

doi: 10.25923/w710-y903



**References**

Keihm, S. J., 1984, Interpretation of the lunar microwave brightness temperature spectrum. Icarus, Vol. 60, No. 3, 568–589, 10.1016/0019-1035(84)90165-9.

Liu, N. and Jin, Y.-Q., 2020, Average Brightness Temperature of Lunar Surface for Calibration of Multichannel Millimeter-Wave Radiometer From 89 to 183 GHz and Data Validation. IEEE Transactions on Geoscience and Remote Sensing, Vol. 59, No. 2, 1345-1354, 10.1109/TGRS.2020.3000230.

Yang, H., Zhou, J., Sun, N., Liu, Q., Leslie, R., Anderson, K. and McCormick, L., 2020, 2-D lunar microwave radiance observations from the NOAA-20 ATMS. IEEE Geoscience and Remote Sensing Letters, 1–4, 10.1109/LGRS.2020.3012518

# NEWS IN THIS QUARTER

## Highlights of the 49th Meeting of the CEOS Working Group on Calibration and Validation

*By Manik Bali (Deputy Director GCC), Akihiko Kuze (Chair WGCV) and Philippe Goryl (Vice Chair WGCV)*

The CEOS Working Group on Calibration and Validation (CEOS-WGCV) met online June 29 – July 2, 2021. The meeting had a comprehensive agenda that spanned topics from the CEOS strategy for the Global Stocktake of the UNFCCC Paris Agreement to CARD4L data sets and WGCV interaction with GSICS to many other topics relevant to the CEOS community. Day 3 of the meeting specifically focused on interaction with GSICS and related topics.

Philippe Goryl, GSICS Executive Panel member and the Vice Chair of WGCV, presented a summary of GSICS activities in the past year. In his presentation, Philippe showed an outline demonstrating that WGCV and GSICS interact directly through the respective subgroups as well at higher level groups such as the CGMS and WMO (Figure 1) and this interaction has greatly benefited each group. Overall, it was noted that there is a lot of complementarity and opportunities for WGCV and GSICS collaboration. For instance, the GSICS Procedure for Product Acceptance has been derived from Quality Assurance for Earth Observation (QA4EO).
Philippe apprised members about the 2021 GSICS Annual Meeting, and then went on to show specific activities and recommendations of each GSICS subgroup. Philip also informed members about the tools developed by GSICS, including some developed by GSICS Data Working Group. Those include Github, GSICS Product Catalog and Notebooks.

Following Philippe's talk, Odele Coddington from LASP, introduced a new Solar Spectrum (TSIS-1) dataset she has developed. This Solar Spectrum, the TSIS-1 HSRS, spans 202–2730 nm at 0.01 to ~0.001 nm spectral resolution with uncertainties of 0.3% between 460 and 2365 nm and 1.3% at wavelengths outside that range. It has now been accepted by GSICS VIS/NIR subgroup as a reference Solar data set for calibrating UV instruments. The TSIS-1 HSRS is a high-accuracy (0.3-1.3%), high-resolution (0.01 nm or better), solar reference spectrum representative of solar minimum between SC 24 & 25. The Solar data set is available for download from https://lasp.colorado.edu/lisird/data/tsis1_hsrs .

J-C Lambert of IASB gave an overview of the H2020 Copernicus Cal/Val

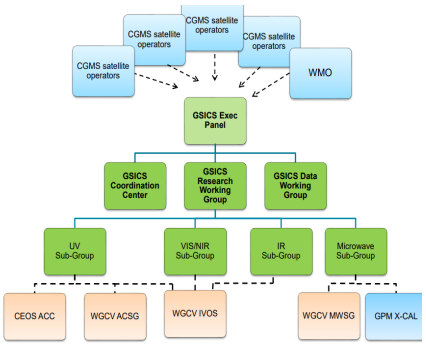


*Figure 1. (Courtesy T. Hewison) above shows the synergy between GSICS and WGCV groups*

Solution (CCVS). The goal of the H2020 CCVS project is to define a holistic solution for all Copernicus Sentinel missions (either operational or planned) to overcome current limitations of Calibration and Validation (Cal/Val) activities. He presented a detailed CAL/VAL plan for Satellites under the Copernicus mission. The deliverables are described at https://ccvs.eu/ .

Members also discussed the Rayleigh Inter-comparison Exercise and asked for expression of interest in this activity.

Presentations and the complete minutes of the meeting can be accessed at https://ceos.org/meetings/wgcv-49/ .

The discussions resulted in the following actions.

doi: 10.25923/w710-y903



| | | |
|---|---|---|
| WGCV 49 04 | Odele to provide comparisons of the TSIS-1 HSRS vs other solar references to support the potential WGCV recommendation of the TSIS-1 HSRS solar spectra. | ASAP to support a WGCV revisit of the recommendation on a dedicated call. |
| WGCV 49 05 | WGCV Chair and Vice Chair to schedule a follow up teleconference on the potential WGCV recommendation of the TSIS-1 HSRS solar spectra. | 2022 |

**Reference:**

https://ceos.org/document_management/Working_Groups/WGCV/Meetings/WGCV-49/WGCV-49_Day-3_Minutes_V1.0.pdf

# Announcements

## AOMSUC-11 & FYUC-2021 to be held online 28-29 October & 1-5 November 2021

*By Allen Huang, SSEC, University of Wisconsin-Madison*

The 11th Asia-Oceania Meteorological Satellite Users' Conference (AOMSUC-11) and the 2021 Fengyun Satellite User Conference (FYUC-2021) will be held virtually on 28-29 October and 1-5 November 2021
Details can be found on the conference web page, including the first announcement and the registration information:
http://www.nsmc.org.cn/conference/fy-suf/2021/index.html
28-29 October, 2-day training event
1-4 November 2021, 4-day joint AOMSUC-11 and FYUC-2021 conference
5 November, 1-day WMO RA-II/RA-V coordination meeting
For information sharing and preserving your contribution, all presentations will be prerecorded and presenters will be expected to upload 15-minute narrated PowerPoint file about two weeks before the conference. Detailed information about how to record PowerPoint presentations and upload your presentation video will be provided in the future announcement.

**Note: There are no fees for conference registration/presentation/attendance.**
Deadline for abstract submission: 30 September 2021
Deadline for presentation upload: 14 October 2021
Deadline for registration: 20 October 2021

Please forward this announcement to all your colleagues to keep the dates aside for participating and continue your great tradition to contribute to our community.

## Workshop Report from SI-Traceable Space-based Climate Observing System (SITSCOS)

*By Tim Hewison (EUMETSAT)*

The GSICS/CEOS workshop on *SI-Traceable Space-based Climate Observing System* was hosted by the National Physical Laboratory, UK, 9-11 September 2019. The workshop report is now published on the CEOS Cal/Val Portal: http://calvalportal.ceos.org/report-and-actions along with the original presentations and overview slides.

# GSICS-Related Publications

Chen, S.; Zheng, X.; Li, X.; Wei, W.; Du, S.; Guo, F. Vicarious Radiometric Calibration of Ocean Color Bands for FY-3D/MERSI-II at Lake Qinghai, China. *Sensors* **2021**, *21*, 139. https://doi.org/10.3390/s21010139

Lebedev S.A., Gusev I.V., International experience in calibration of satellite altimetry data on the stationary and temporary calibration sites, Sovremennye problemy distantsionnogo zondirovaniya Zemli iz kosmosa, 2021, Vol. 18, No. 2, pp. 18–35 (in Russian), DOI: 10.21046/2070-7401-2021-18-2-18-35.

Lili Qie, Zhengqiang Li, Sifeng Zhu, Hua Xu, Yisong Xie, Rui Qiao, Jin Hong, and Bihai Tu, "In-flight radiometric and polarimetric calibration of the Directional Polarimetric Camera onboard the GaoFen-5 satellite over the ocean," Appl. Opt. 60, 7186-7199 (2021): 10.1364/AO.422980.

Liu, Li, Tingting Shi, Hailiang Gao, Xuewen Zhang, Qijin Han, and Xinkai Hu. 'Long-Term Cross Calibration of HJ-1A CCD1 and Terra MODIS Reflective Solar Bands'. *Scientific Reports* 11, no. 1 (1 April 2021): 7386. https://doi.org/10.1038/s41598-021-86619-y.

J. Lu, T. He, S. Liang and Y. Zhang, "An Automatic Radiometric Cross-Calibration Method for Wide-Angle Medium-Resolution Multispectral Satellite Sensor Using Landsat Data," in *IEEE Transactions on Geoscience and Remote Sensing*, doi: 10.1109/TGRS.2021.3067672.

M. Kang *et al*., "Characteristics of the Spectral Response Function of Geostationary Environment Monitoring Spectrometer Analyzed by Ground and In-Orbit Measurements," in *IEEE Transactions on Geoscience and Remote Sensing*, doi: 10.1109/TGRS.2021.3091677.Saunders, R. W., T. A. Blackmore, B. Candy, P. N. Francis and T. J. Hewison, "Ten Years of Satellite Infrared Radiance Monitoring With the Met Office NWP Model," in *IEEE Transactions on Geoscience and Remote Sensing*, vol. 59, no. 6, pp. 4561-4569, June 2021, doi: 10.1109/TGRS.2020.3015257.

X. Li, Z. Ye, Y. Ye and X. Hu, "A Convolutional Neural Network-Based Relative Radiometric Calibration Method," in *IEEE Transactions on Geoscience and Remote Sensing*, doi: 10.1109/TGRS.2021.3105182.

Y. Liu *et al*., "A Spectrum Extension Approach for Radiometric Calibration of the Advanced Hyperspectral Imager Aboard the Gaofen-5 Satellite," in *IEEE Transactions on Geoscience and Remote Sensing*, doi: 10.1109/TGRS.2021.3083707.

## Submitting Articles to the GSICS Quarterly Newsletter:

The GSICS Quarterly Press Crew is looking for short articles (800 to 900 words with one or two key, simple illustrations), especially related to calibration / validation capabilities and how they have been used to positively impact weather and climate products. Unsolicited articles may be submitted for consideration anytime, and if accepted, will be published in the next available newsletter issue after approval / editing. Please send articles to manik.bali@noaa.gov.

## With Help from our friends:

The GSICS Quarterly Editor would like to thank Dave Doelling (NASA), Sriharsha Madhavan (SSAI), Cheng-Zhi Zou (NOAA) and Lawrence Flynn (NOAA) for reviewing articles in this issue. Thanks are due to Jan Thomas (NOAA) for helping with 508 compliance.

doi: 10.25923/w710-y903





**Published By**

GSICS Coordination Center
NOAA/NESDIS/STAR NOAA
Center for Weather and Climate Prediction,
5830 University Research Court
College Park, MD 20740, USA

CISESS
5825 University Research Court, Suite 4001,
University of Maryland, College Park, MD 20740-3823